Int. J. Heat Mass Transfer. Vol. 36, No. 11, pp. 2913–2925, 1993
Printed in Great Britain

0017–9310/93 $6.00+0.00

Scaling of the laminar natural-convection flow in a heated square cavity

R. A. W. M. HENKES and C. J. HOOGENDOORN
J. M. Burgers Centre for Fluid Mechanics, Faculty of Applied Physics, Delft University of Technology, P.O. Box 5046, 2600 GA Delft, The Netherlands

(*Received* 10 *June* 1992)

Abstract—The steady laminar natural-convection flow of air and water in a square heated cavity is calculated for increasingly large Rayleigh number. The flow is calculated by solving both the Navier–Stokes equations and the boundary-layer equations. The results are used to determine the proper scalings of the flow in the different asymptotic flow regions: vertical boundary layers, core region, corner region and horizontal boundary layers. In particular the scalings according to the Navier–Stokes equations agree with the asymptotic model for the core and vertical boundary layers as proposed by Gill [*J. Fluid Mech.* **26**, 515–536 (1966)].

1. INTRODUCTION

NATURAL-CONVECTION flows play a role in different technical applications, like solar collectors, climate conditioning of rooms, isolation by double glazing, heat removal in micro electronics and cooling of nuclear reactors. Therefore natural-convection flows in rectangular geometries differentially heated over the vertical side have become a classical heat-transfer subject. The present study concentrates on the structure of the steady laminar flow in a square cavity for increasingly large Rayleigh number.

Actually the natural-convection problem is characterized by two numbers, the Rayleigh number and the Prandtl number. The proper scalings of the problem are those scalings which make the scaled solution independent of the Rayleigh number if the Rayleigh number is increased to infinity. In the limit of an infinitely large Rayleigh number some terms disappear from the Navier–Stokes formulation, which now simplifies to an asymptotic description. The proper scalings are given by the asymptotic description (for example the boundary-layer equations). In the cavity there are several asymptotic regions, each with its own proper scalings.

Elder [1] and Gill [2] have formulated some ideas about the asymptotic equations, and hence the proper scalings, of the steady laminar flow in the cavity with an adiabatic floor and ceiling, that is heated from the vertical side. They distinguish a core and boundary layers along the vertical walls. The core is thermally stratified and has a zero vertical flow. Gill assumes that for large Rayleigh numbers the Navier–Stokes equations reduce to boundary-layer equations. He largely simplified the boundary-layer equations and determined the stratification in such a way that the stream function at the edge of the boundary layer was symmetric with respect to the position of half the cavity height.

In order to verify Gill's asymptotic theory, in the present study the asymptotic structures, with the proper scalings, are derived by calculating the steady laminar Navier–Stokes flow in the two-dimensional square cavity for air up to a Rayleigh number of 10^9 and for water up to $Ra = 10^{11}$. Further, the thermal stratification as calculated in the large-Rayleigh-number Navier–Stokes solution is used as a boundary condition to solve the boundary-layer equations.

2. STEADY NAVIER–STOKES AND BOUNDARY-LAYER EQUATIONS

We consider the flow in a square cavity, that has a hot left vertical wall (temperature T_h) and a cold right vertical wall (T_c). The floor and ceiling are both adiabatic ($\partial T/\partial y = 0$). The height of the cavity is H. The flow is described by the Navier–Stokes equations under the Boussinesq approximation:

$$\frac{\partial u}{\partial x}+\frac{\partial v}{\partial y}=0$$

$$u\frac{\partial u}{\partial x}+v\frac{\partial u}{\partial y}=-\frac{1}{\rho}\frac{\partial p}{\partial x}+\nu\left(\frac{\partial^2 u}{\partial x^2}+\frac{\partial^2 u}{\partial y^2}\right)$$

$$u\frac{\partial v}{\partial x}+v\frac{\partial v}{\partial y}=-\frac{1}{\rho}\frac{\partial p}{\partial y}+g\beta(T-T_0)+\nu\left(\frac{\partial^2 v}{\partial x^2}+\frac{\partial^2 v}{\partial y^2}\right)$$

$$u\frac{\partial T}{\partial x}+v\frac{\partial T}{\partial y}=\frac{\nu}{Pr}\left(\frac{\partial^2 T}{\partial x^2}+\frac{\partial^2 T}{\partial y^2}\right). \quad (1)$$

Here x and y are the horizontal and vertical coordinates, respectively, with the corresponding velocity components u and v; T is the temperature; p is the pressure; ρ is the (constant) density; g is the gravitational acceleration; β is the coefficient of thermal expansion; ν is the molecular viscosity and Pr is the Prandtl number.

NOMENCLATURE

g	gravitational acceleration
H	height of cavity
Nu	Nusselt number for cavity, $-(H/\Delta T)(\partial T/\partial x)_w$
$\overline{Nu}$	averaged Nusselt number in cavity. $\int_0^1 Nu\, \mathrm{d}(y/H)$
p	pressure
Pr	Prandtl number
Ra	Rayleigh number, $g\beta\Delta TH^3Pr/\nu^2$
S	gradient of thermal stratification in cavity centre, $(H/\Delta T)(\partial T/\partial y)$
T	temperature
ΔT	characteristic temperature difference for cavity, $T_h - T_c$
T_c	temperature of cold cavity wall
T_h	temperature of hot cavity wall
u	horizontal velocity component
u_0	velocity scale for cavity, $(g\beta\Delta T\nu)^{1/3}$
v	vertical velocity component
x	horizontal coordinate
y	vertical coordinate.

Greek symbols

β	coefficient of thermal expansion
ν	molecular kinematic viscosity
ρ	density
ψ	stream function, $u = -\partial\psi/\partial y$, $v = \partial\psi/\partial x$
ψ_c	stream function at centre of cavity.

Subscripts

max	maximum of a quantity
w	wall condition
∞	environment condition.

The variables are nondimensionalized with the length scale x_0, the velocity scale u_0, the characteristic temperature T_0, and the characteristic temperature difference ΔT:

$$\left\{\frac{u}{u_0}, \frac{v}{u_0}, \frac{T-T_0}{\Delta T}, \frac{p}{\rho u_0^2}\right\} = f\left\{\frac{x}{x_0}, \frac{y}{x_0}, \frac{x_0 g\beta\Delta T}{u_0^2}, \frac{\nu}{u_0 x_0}, Pr\right\}. \quad (2)$$

The geometry and boundary conditions for the temperature determine length and temperature scales: $x_0 = H$, $T_0 = T_c$, $\Delta T = T_h - T_c$. The zero boundary condition for the velocity does not define a velocity scale. Therefore the velocity scale can be freely constructed with the help of H and the coefficients $g\beta\Delta T$ and ν; a possible choice is $u_0 = (g\beta\Delta T\nu)^{1/3}$. Because of the free choice of the velocity scale, the number of independent variables in equation (2) reduces by one,

$$\left\{\frac{u}{u_0}, \frac{v}{u_0}, \frac{T-T_c}{\Delta T}, \frac{p}{\rho u_0^2}\right\} = f\left\{\frac{x}{H}, \frac{y}{H}, Ra, Pr\right\}. \quad (3)$$

In this relation the Rayleigh number is defined as $Ra = g\beta\Delta TH^3Pr/\nu^2$. Hence, the dimensionless Navier–Stokes solution depends on only two characteristic numbers, namely the Rayleigh number and the Prandtl number.

With the large-Rayleigh-number Navier–Stokes solutions in the square cavity it will be checked whether the hot vertical wall of the cavity can be considered as a part of a semi-infinite hot vertical plate, placed in a stagnant, stratified environment. More precisely, in the asymptotic limit of $Ra \to \infty$, the Navier–Stokes description along the hot wall is expected to simplify to the boundary-layer equations

$$\frac{\partial u}{\partial x} + \frac{\partial v}{\partial y} = 0$$

$$u\frac{\partial v}{\partial x} + v\frac{\partial v}{\partial y} = -\frac{1}{\rho}\frac{\mathrm{d}p}{\mathrm{d}y} + g\beta(T - T_c) + \nu\frac{\partial^2 v}{\partial x^2}$$

$$u\frac{\partial T}{\partial x} + v\frac{\partial T}{\partial y} = \frac{\nu}{Pr}\frac{\partial^2 T}{\partial x^2}$$

$$x = 0: u = v = 0, \quad T = T_h$$

$$x \to \infty: v = 0, \quad T = T_\infty(y). \quad (4)$$

Because for $x \to \infty$ the temperature converges to $T_\infty(y)$ and the convection and the diffusion terms vanish, the pressure in the boundary-layer equations (4) is only the hydrostatic pressure, which directly follows from the prescribed stratification:

$$\frac{p(x, y)}{\rho g\beta\Delta TH} = \int_0^y \frac{T_\infty(y') - T_c}{\Delta TH}\,\mathrm{d}y' + \frac{p^*}{\rho g\beta\Delta TH} \quad (5)$$

where p^* is a fixed pressure level. The solution of the boundary-layer equations does not explicitly depend on the Rayleigh number if it is scaled according to

$$\left\{\frac{u}{u_0}Ra^{1/2}, \frac{v}{u_0}Ra^{1/6}, \frac{T-T_c}{\Delta T}, \frac{p}{\rho u_0^2}Ra^{1/3}\right\} = f\left\{\frac{x}{H}Ra^{1/4}, \frac{y}{H}, Pr\right\}. \quad (6)$$

3. NUMERICAL METHOD

In order to numerically determine the Navier–Stokes solution, equations (1) are discretized with the

well-known finite-volume method on a staggered grid. The convection terms are discretized with the central scheme. The domain is covered with a nonequidistant grid, having a concentration of grid lines along the walls. The u-grid points are positioned in the x-direction according to

$$\frac{x_i}{H} = \frac{i}{i_{\max}} - \frac{1}{2\pi}\sin\left(2\pi\frac{i}{i_{\max}}\right) \quad i = 0, 1, \ldots, i_{\max}. \quad (7)$$

The same spacing is used for the v-grid points in the y-direction. The pressure is updated with the SIMPLE pressure-correction method. A line Gauss–Seidel iteration is used to solve both the transport variables (u, v and T) and the pressure correction. Convergence of the Navier–Stokes solution becomes more difficult the larger the Rayleigh number is, and relaxation is required to prevent divergence. Part of the convergence problems are expected to be due to the calculation of the pressure in the boundary layers along the vertical walls. In contrast with the Navier–Stokes equations, the boundary-layer equations do not have a transport equation for the normal velocity component u, but the u-component directly follows from the continuity equation. This boundary-layer feature is not reflected by the Navier–Stokes solver, which determines a pressure correction via the continuity equation and which determines the u-component via the u-transport equation.

The boundary-layer equations are parabolic as long as the environment is isothermal or unstably stratified ($dT_\infty/dy \leqslant 0$). Because of this parabolic character, it is more suitable to modify the position of some of the grid points used to discretize the elliptic Navier–Stokes equations when the boundary-layer equations are solved. To discretize the boundary-layer equations we take the same grid points for v as in the discretization of the Navier–Stokes equations, but the grid points for T are moved to the v-grid points and the grid points for u are only staggered with respect to the v-grid points in the x-direction. Further, a first-order upwind discretization is used for the convection in the y-direction. In this way only one sweep from the beginning to the end of the domain (in which the updating process at a line is repeated until a convergence criterion is satisfied) is required to solve the parabolic boundary-layer equations. If the temperature stratification is stable ($dT_\infty/dy > 0$), regions of flow reversal and temperature deficit appear, implying that the boundary-layer equations lose their parabolic character and become elliptic. Due to this elliptic character, even on the modified grid repeated sweeps have to be made. The flow reversal, however, is small and the equations are still nearly parabolic. Therefore also for the stable stratification the line-updating process in each sweep on the modified grid is repeated until convergence at that line is reached. This contrasts the Navier–Stokes solver, in which only one line-updating is made in each sweep.

4. GILL'S ASYMPTOTIC FORMULATION

Since Prandtl [3] derived the boundary-layer equations, and actually introduced the mathematical technique of asymptotic series (singular perturbation theory) to solve flow problems, a large literature on this subject has been established. The asymptotic theory searches for the proper scalings in the asymptotic limit of an infinitely large Rayleigh number, and it derives the corresponding asymptotic equations. These scalings can be different in different regions, and the asymptotic solutions have to be matched according to a certain matching principle. The asymptotic solution holds exactly in the limit $Ra \to \infty$, and can be used as a good approximation of the Navier–Stokes solution for a large, but finite, Rayleigh number.

The asymptotic theory for the natural-convection flow in cavities is still in development. Ostrach [4, 5] has given reviews. Two basic configurations have been considered in the literature, the rectangular cavity and the horizontal cylinder, for two basic modes, heating from the vertical side and heating from below. For large Rayleigh numbers there seems to be a core with boundary layers along the heated walls. There has been some doubt on the right structure of the core flow; Batchelor [6] suggested an isothermal core with constant vorticity for the configuration with heating from the vertical side. At the moment it seems (experiments Elder [1], theoretical considerations Ostrach and Hantman [7], and different numerical studies including the present one) that the core becomes isothermal and rotating if the cavity is heated from below, whereas it becomes thermally stratified and almost stagnant with horizontal streamlines if the cavity is heated from the vertical side.

The vertical boundary layers and the core in rectangular cavities have been calculated by Gill [2] for infinitely large Rayleigh and Prandtl numbers. He assumes that the core is stratified and has horizontal streamlines. Along the vertical walls Gill approximately solves the boundary-layer equations (4) by linearizing them. After linearization the boundary-layer equations reduce to an ordinary differential equation in x, in which the y-coordinate appears as a parameter only. The core flow and boundary-layer flow are matched by the condition that the temperature and the normal velocity at the edge of the boundary layer are equal to the temperature and velocity in the core. The solution of equations (1), under the given boundary conditions, is centro-symmetric with respect to the centre of the cavity:

$$T(x,y) - T(H/2, H/2) = T(H/2, H/2) - T(H-x, H-y)$$
$$u(x,y) = -u(H-x, H-y). \quad (8)$$

Because of the assumption that the streamlines are horizontal in the core, it also follows that the normal velocity at the edge of the boundary layer along both vertical walls is anti-symmetric around $y = H/2$. This symmetry condition dictates how the asymptotic flow in the core and in the boundary layer interact: the

stratification in the core has to be such that the normal velocity at the outer edge of the boundary layer is anti-symmetric. Using the symmetry conditions the linearized boundary-layer solution and the core solution can be determined up to a constant. Gill determines this constant by assuming that the vertical entrainment of mass at the ceiling ($y = H$) equals zero. A modified procedure to determine this constant has been proposed by Bejan [8]. He applies the condition that the vertical heat flux through the ceiling is zero. The vertical flux consists of a convection and a diffusion contribution, which are calculated with Gill's approximation of the boundary-layer solution. The constant turns out to be a coefficient that depends on the Rayleigh number; the coefficient converges to Gill's constant in the limit $Ra \to \infty$. From an asymptotic point of view one might doubt the significance of Bejan's correction. The boundary-layer solution is used to calculate the y-diffusion, which actually was neglected when the boundary-layer equations were derived from the Navier–Stokes equations. Therefore Bejan's correction on Gill's constant is a second-order asymptotic effect, which can only be expected to be the right second-order correction if it has been determined in combination with second-order boundary-layer equations and core effects. Graebel [9] extended Gill's analysis to variable Prandtl numbers. Blythe *et al.* [10] repeated Gill's analysis (only for the limit $Pr \to \infty$); instead of linearizing the boundary-layer equations, they accurately solved Gill's asymptotic formulation with a numerical method.

Gill's asymptotic structure will be verified by comparison with large-Rayleigh-number Navier–Stokes solutions. In the sequel the mentioned approximation, including Graebel's finite-Prandtl-number correction, will be referred to as the *approximation* of Gill's formulation and the numerical solution of Blythe *et al.* will be referred to as the *exact* solution of Gill's formulation.

5. NAVIER–STOKES SOLUTIONS

Steady, laminar Navier–Stokes solutions in the cavity are determined for air ($Pr = 0.71$) up to $Ra = 10^9$ and for water ($Pr = 7.0$) up to $Ra = 10^{11}$. Benchmark numerical results were obtained by de Vahl Davis [11] for air up to $Ra = 10^6$. Recently Le Quéré [12] revisited these benchmark results, and he also added benchmark results for two new cases: air at $Ra = 10^7$ and air at $Ra = 10^8$. To discretize the equations de Vahl Davis used a finite-difference method and Le Quéré used a spectral method.

Most of the present calculations were made on a 60×60 grid. For Rayleigh numbers up to 10^4 an equidistant grid was used, whereas for larger Rayleigh numbers the nonequidistant grid (7) was used. In order to verify the accuracy for larger Rayleigh numbers, we refined the grid up to 120×120 points for air at $Ra = 10^6$ and for air at $Ra = 10^8$. Table 1 summarizes the results at $Ra = 10^6$ for several quantities: the averaged heat transfer through the hot vertical wall ($\overline{Nu}$, in which Nu is the Nusselt number defined by $-(H/\Delta T)(\partial T/\partial x)_w$), the gradient of the thermal stratification in the centre ($S = (H/\Delta T)\partial T/\partial y$), the vertical velocity maximum at half the cavity height (v_{max}) and the horizontal velocity maximum at half the cavity width (u_{max}). The results, in particular at the finest grids, are in very good agreement with the benchmark results of de Vahl Davis [11], but the agreement with the revised benchmark results of Le Quéré [12] is even better. Table 2 refines the grid for $Ra = 10^8$ and also compares different discretizations for the convection (central, hybrid, first-order upwind). By strong grid refinement Le Quéré can convince that his solution at $Ra = 10^8$ is indeed very accurate and that it can be used as a benchmark solution. He does not give a benchmark value for the stratification. Therefore we use our value at the 120×120 grid with the central scheme as a reference value for S; changes in S on the refined grids are smallest with the central scheme, suggesting that this scheme has the highest accuracy. Differences between the schemes are small, with exception of the stratification: the hybrid scheme and the upwind scheme considerably underpredict the stratification at the coarser grids. Comparison with the benchmark solution at $Ra = 10^8$ shows that our values for the wall-heat transfer and for the vertical velocity maximum at the finest grids are very accurate. The accuracy of our horizontal velocity maximum is somewhat smaller. Relaxation is required to prevent divergence of the numerical iteration process: convergence becomes slower in the sequence upwind scheme, hybrid scheme and central scheme. For air at $Ra = 10^9$ a converged solution with the central

Table 1. Accuracy of the solution for air at $Ra = 10^6$ (central scheme)

Study	Grid	S	$\overline{Nu}\,Ra^{-1/4}$	$\frac{v_{max}}{\sqrt{(g\beta\Delta TH)}}$	$\frac{u_{max}}{(g\beta\Delta Tv)^{1/3}}$
Present	15×15	0.9780	0.2773	0.2977	0.8422
	30×30	0.9367	0.2782	0.2658	0.8174
	60×60	0.9190	0.2789	0.2633	0.8145
	120×120	0.9144	0.2790	0.2621	0.8144
de Vahl Davis	—	—	0.2783	0.2603	0.8121
Le Quéré	—	—	0.2791	0.2618	0.8146

Table 2. Accuracy of the solution for air at $Ra = 10^8$

Scheme	Grid	S	$\overline{Nu}\, Ra^{-1/4}$	$\frac{v_{max}}{\sqrt{(g\beta\Delta TH)}}$	$\frac{u_{max}}{(g\beta\Delta Tv)^{1/3}}$
Central	15×15	0.9336	0.3134	0.3790	0.6446
	30×30	0.9908	0.2988	0.2827	0.7436
	60×60	0.9942	0.3014	0.2657	0.7421
	120×120	0.9943	0.3020	0.2646	0.8231
Hybrid	15×15	0.7732	0.2971	0.3712	0.9209
	30×30	0.9297	0.2937	0.2836	0.7670
	60×60	0.9714	0.2989	0.2667	0.7776
	120×120	0.9808	0.3010	0.2649	0.7937
Upwind	15×15	0.5976	0.2995	0.3557	1.111
	30×30	0.8369	0.3014	0.2767	0.9139
	60×60	0.9121	0.3035	0.2633	0.8619
	120×120	0.9502	0.3034	0.2633	0.8321
Le Quéré	—	—	0.3023	0.2637	0.8714

scheme could no longer be obtained and the hybrid scheme had to be used.

Streamlines of the Navier–Stokes solution for air at increasing Rayleigh number are shown in Fig. 1(a). Streamlines are isolines of the stream function ψ, which is defined as $u = -\partial\psi/\partial y$, $v = \partial\psi/\partial x$ and $\psi = 0$ at the wall. Special points in the streamline patterns are the stagnant points, that is, the points where $u = v = 0$. As indicated in Fig. 1(b), a stagnant point can either be a centre or a saddle. The stagnant points define the topological structure of the flow; the streamlines through the saddles give the dividing

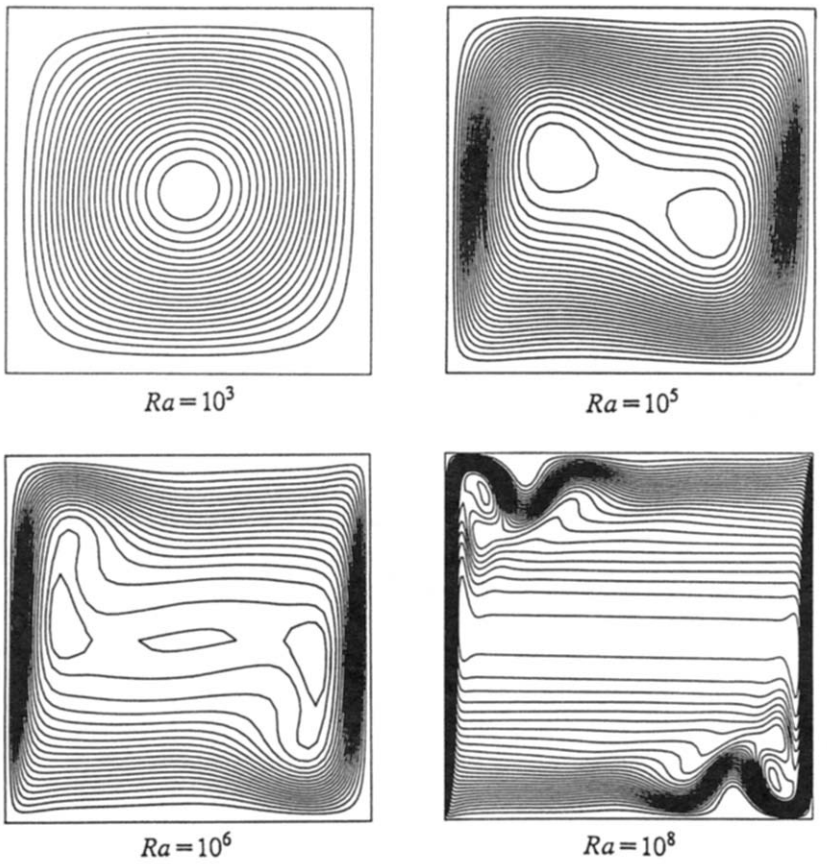

FIG. 1. Structure of the Navier–Stokes solution for increasing Rayleigh number; (a) streamlines for air, (b) topology.

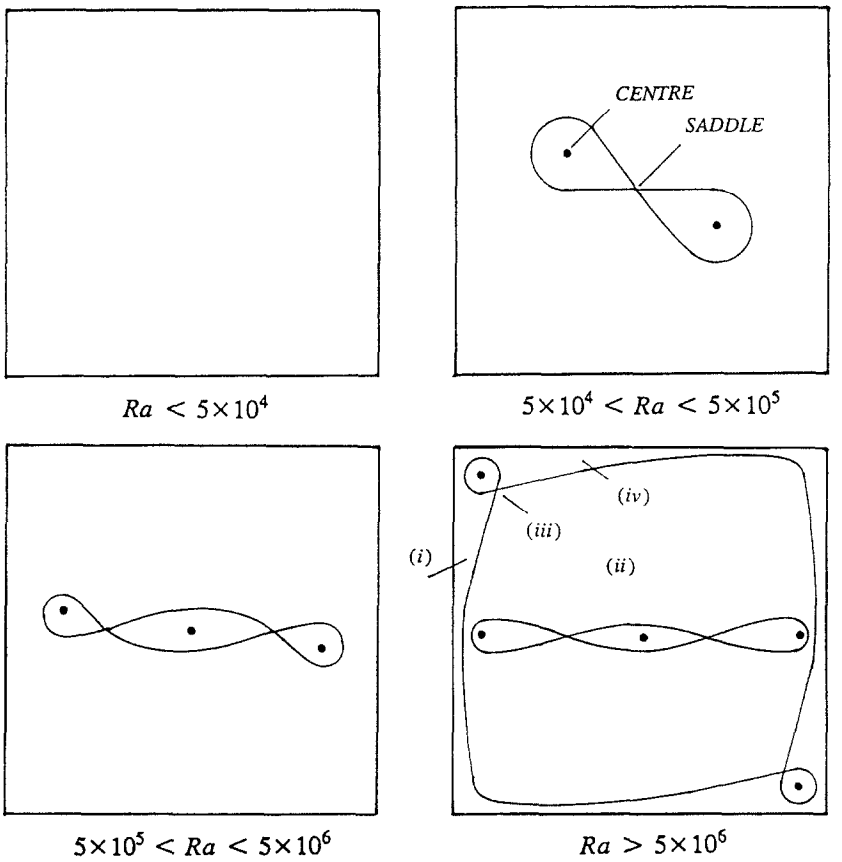

FIG. 1.—*Continued.*

streamlines of the flow. With the help of the stagnant points, the following ranges can be distinguished (the streamlines are centro-symmetric with respect to $x = y = H/2$):

I. $Ra < 5 \times 10^4$; one centre at $x = y = H/2$, with unicellular, clockwise rotating flow.
II. $5 \times 10^4 < Ra < 5 \times 10^5$; the centre has split up in a saddle, at $x = y = H/2$, and two new centres, forming two clockwise rotating rolls.
III. $5 \times 10^5 < Ra < 5 \times 10^6$, the saddle at $x = y = H/2$ has further split up in a centre and two new saddles, giving a total of three clockwise rotating rolls.
IV. $Ra > 5 \times 10^6$; a centre-saddle combination is formed in the left upper and right lower corner, with fast clockwise rotating fluid (vortices). This corner vortex does appear only for air. It does *not* appear for water up to $Ra = 10^{11}$, which was the largest Rayleigh number we calculated.

As indicated in Fig. 1(b), four asymptotic regions can be distinguished in the last streamline pattern: (i) vertical boundary layer along the heated wall, (ii) core region, (iii) corner region, (iv) horizontal layer.

6. SOLUTION OF THE BOUNDARY-LAYER EQUATIONS

Figure 2 shows the isotherms in the Navier–Stokes solution for air at increasing Rayleigh number. For very small Rayleigh numbers there is only conduction, giving a temperature which only depends on the x-coordinate ($S = 0$). For increasing Rayleigh number the temperature in the core of the cavity becomes stratified, that is, the temperature depends only on the vertical coordinate y. The stratification at half the cavity width is shown in Figs. 3(a) and (b), for air and water, respectively. The stratification at the centre (S) is shown in Fig. 3(c). Part of the curve in Fig. 3(c) is broken to indicate that the steady solution for these large Rayleigh numbers is physically unstable (see, for example, Paolucci and Chenoweth [13]). Figure 3 shows that for $Ra \to \infty$ the core stratification converges to a limit state; the limit stratification for air is roughly twice the limit stratification for water.

With the limit stratification of the Navier–Stokes solution prescribed as a boundary condition at the outer edge, the boundary-layer equations (4) were solved for air (actually the stratification for $Ra = 10^8$ was taken). For $y \downarrow 0$ the solution of the boundary-

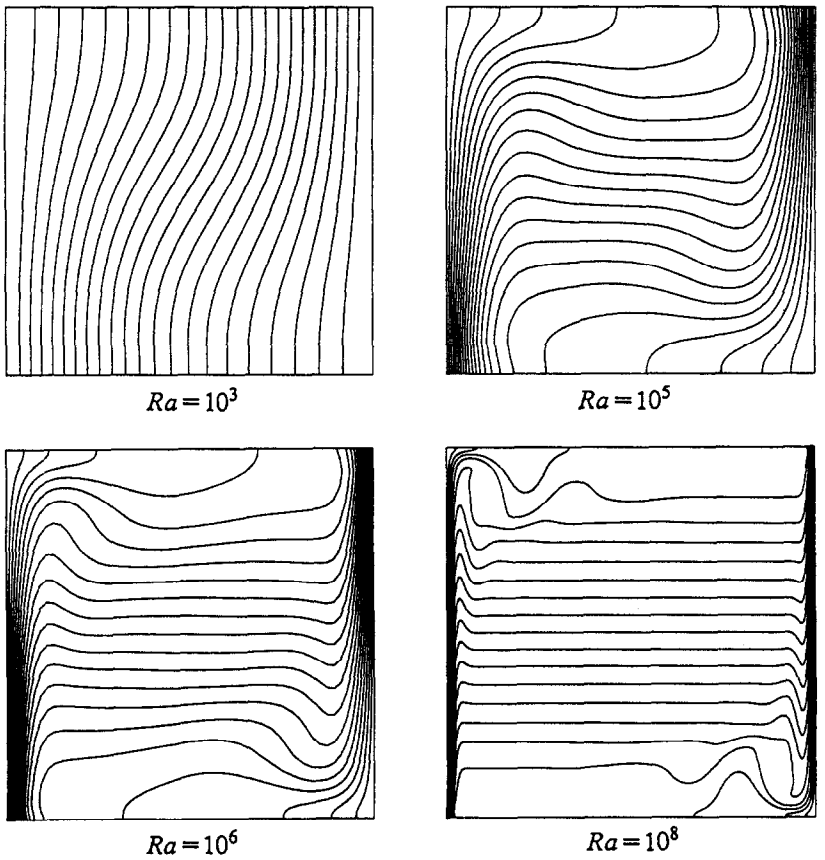

FIG. 2. Isotherms in the Navier–Stokes solution for increasing Rayleigh number (air).

layer equations simplifies to Ostrach's [14] similarity solution. This solution was used as a boundary condition at the leading edge. As shown in the previous section, regions with flow reversal and temperature deficit are found in the outer part of the boundary layer if the environment is stably stratified. This implies also that a boundary condition is required at the end of the boundary layer at $y = H$. Because the solution at $y = H$ is not known beforehand, the calculation was extended to $y > H$, using the outer-edge temperature $T_\infty(y) = T_\infty(H)$ in this range. For $y \gg H$ the boundary layer returns to Ostrach's similarity solution. The outer edge of the boundary layer in the computational domain was taken far enough to have a negligible effect on the development of the boundary layer (namely at $(x/H)\ Ra^{1/4} = 40$). Forty grid points were used in the y-range $0 < y \leqslant H$. The same number of grid points was used in the x-direction. Calculations on 80×80 grids gave only very small changes.

The wall-heat transfer in the boundary-layer solution and in the Navier–Stokes solution for increasing Rayleigh number are compared in Fig. 4(a) for air: the wall-heat transfer in the Navier–Stokes solution converges to the value of the boundary-layer solution in the limit $Ra \to \infty$. In particular in Fig. 4(b) it is checked that the wall-heat transfer $-(\partial T/\partial x)_w$ in the Navier–Stokes solution for large Rayleigh numbers scales with $(\Delta T/H)Ra^{1/4}$, which agrees with the boundary-layer scaling (6). Finite-Rayleigh-number effects are restricted to the corners at $y \downarrow 0$ and at $y \uparrow H$. If the Rayleigh number is increased, the position of the maximum in the Navier–Stokes wall-heat transfer moves to $y/H = 0$, and for small y values beyond this maximum the wall-heat transfer follows Ostrach's similarity solution,

$$\lim_{Ra\to\infty} Nu\, Ra^{-1/4} = C^*(y/H)^{-1/4} \lim_{Ra\to\infty} \left(\frac{T_h - T(H/2,0)}{\Delta T}\right)^{5/4} \quad (9)$$

with $C^* = 0.387$ for air and 0.459 for water. Here the infinite-Rayleigh-number limit of $(T_h - T(H/2,0))/\Delta T$ is found by extrapolation of the results for the largest calculated Rayleigh numbers to infinity, which gives about 0.86 for air and about 0.91 for water.

In Fig. 5(a) the stream function at the outer edge of the boundary-layer solution for air is compared with the Navier–Stokes stream function at $x = H/2$ for increasing Rayleigh number. The convergence of the Navier–Stokes stream function to the boundary-

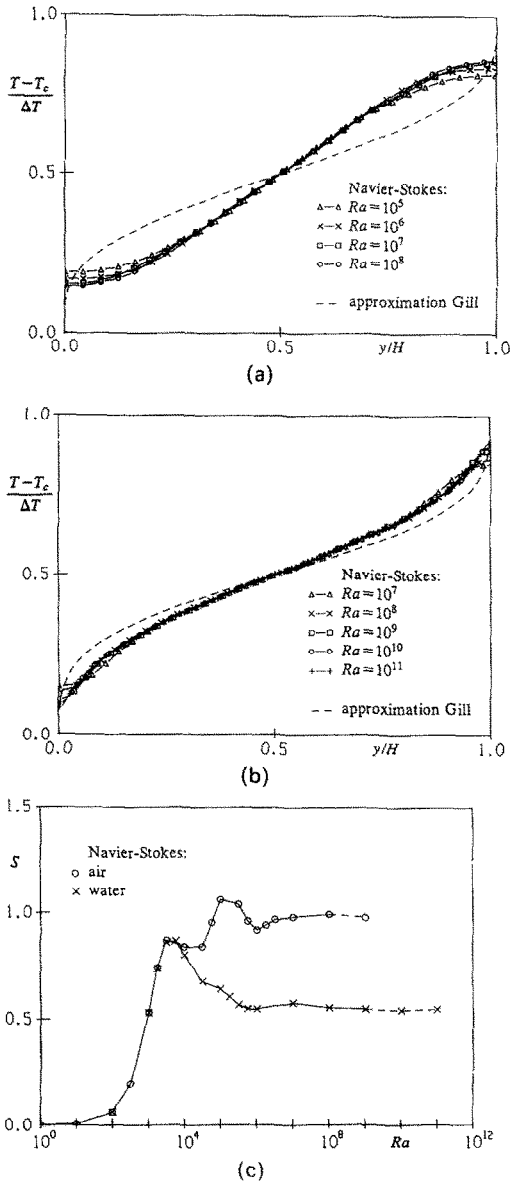

FIG. 3. Stratification in the core; (a) at $x = H/2$ for air, (b) at $x = H/2$ for water, (c) at the centre.

layer solution is only clear for y-values up to $H/2$. In particular in Fig. 5(b) it is checked that the Navier–Stokes stream function at the centre (ψ_c) scales with $u_0 H Ra^{-1/12}$, which agrees with the boundary-layer scaling (6) (see also next section). For $y > H/2$ the deviation of the boundary-layer solution from the Navier–Stokes solution is large and the stream function in the boundary-layer solution is not symmetric around $y = H/2$. In order to verify the sensitivity of the stream function to the stratification, the boundary-layer equations were solved for different stratifications as sketched in Fig. 6(a); both the linearized $Ra = 10^8$ Navier–Stokes stratification and the linearized stratification with a sinus perturbation were used. Changing the stratification has a small influence on the wall-heat transfer (Fig. 6(b)), but it has a large influence on the stream function for $y > H/2$ (Fig.

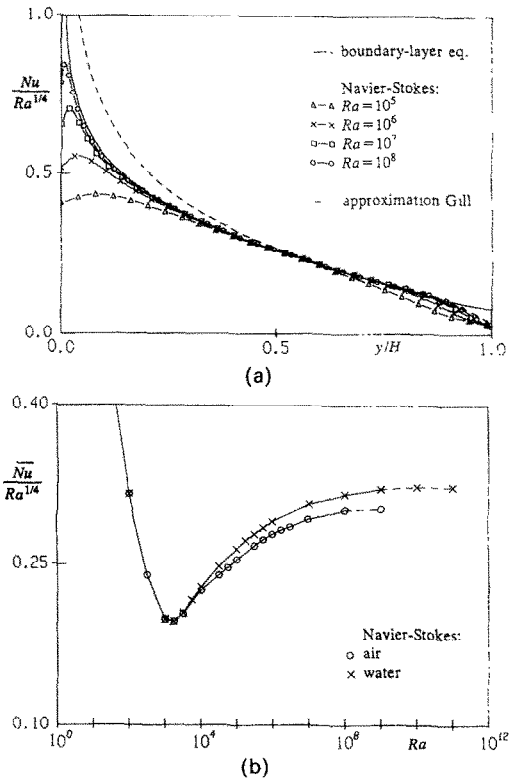

FIG. 4. Wall-heat transfer; (a) for air, (b) averaged wall-heat transfer.

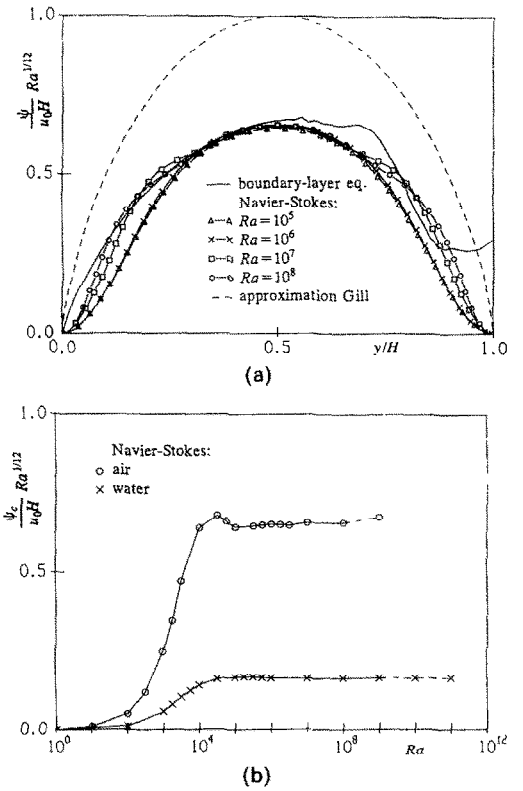

FIG. 5. Stream function; (a) at $x = H/2$ for air, (b) at the centre.

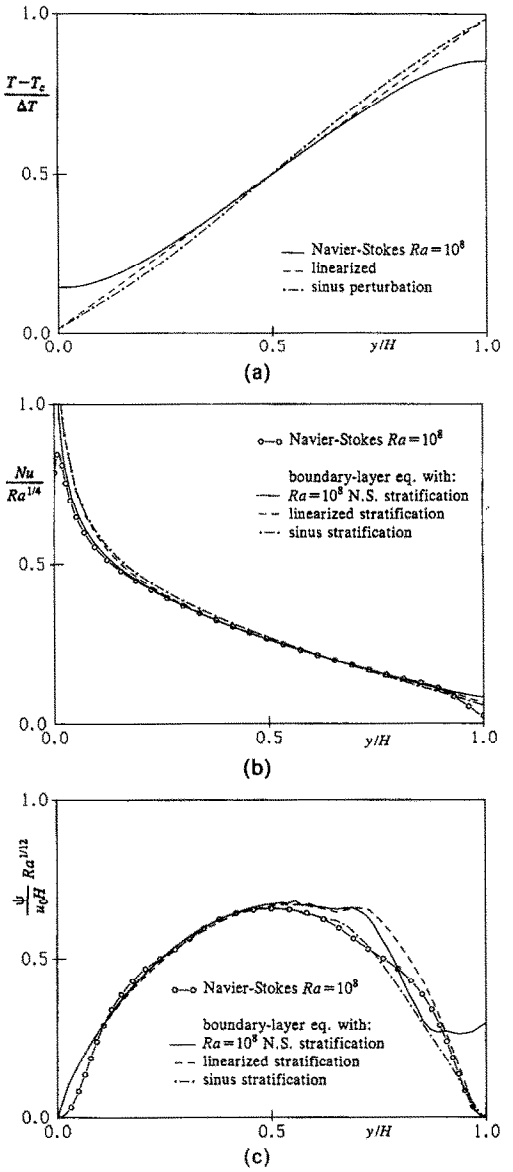

FIG. 6. Sensitivity of the boundary-layer solution for air to the stratification; (a) core temperatures checked, (b) wall-heat transfer, (c) stream function at the edge.

6(c)). The linearized stratification removes the deviation in the stream function with the Navier–Stokes solution close to the ceiling, and the sinus perturbation makes the stream function practically symmetric. The large sensitivity of the stream function to the temperature stratification suggests that the interaction between the core solution and the boundary-layer solution has to be taken into account. This is precisely what is done in the asymptotic description of Gill: as described in Section 4, he uses the interaction principle of symmetry to couple the stratification to the boundary-layer equations. Gill does not prescribe a fixed stratification, but the stratification is part of the calculation. It remains to be checked that applying the symmetry interaction in the present boundary-layer approach (for example by setting up an iteration process that corrects the prescribed stratification until a symmetric stream function at the outer edge of the boundary-layer solution is found) gives a stratification which is close to the calculated large-Rayleigh-number Navier–Stokes limit.

Table 3. Comparison of the asymptotic behaviour

(a) Air

Formulation	S	$\overline{Nu}\,Ra^{-1/4}$	$\frac{\psi_c}{u_0 H Ra^{-1/12}}$
Navier–Stokes	0.99	0.30	0.66
Boundary-layer equations	0.99	0.31	0.67
Gill-exact	0.52	0.32	0.74
Gill-approximation	0.49	0.36	1.0
Similarity solution	0.00	0.22	1.17

(b) Water

Formulation	S	$\overline{Nu}\,Ra^{-1/4}$	$\frac{\psi_c}{u_0 H Ra^{-1/12}}$
Navier–Stokes	0.55	0.32	0.16
Boundary-layer equations	—	—	—
Gill-exact	0.52	0.32	0.16
Gill-approximation	0.42	0.36	0.21
Similarity solution	0.00	0.26	0.65

Table 3 compares some asymptotic limits in the Navier–Stokes solution with the boundary-layer solution, Gill's formulation and Ostrach's similarity solution. The boundary-layer solution is found by prescription of the Navier–Stokes stratification, Gill's formulation uses interaction to calculate the stratification, and Ostrach's similarity solution applies a zero stratification to the boundary-layer equations. The fixed outer-edge temperature in the similarity solution was chosen as $(T_h+T_c)/2$. The agreement of the wall-heat transfer and the stream function at the centre between the Navier–Stokes solution and the boundary-layer solution is good, as just discussed. The agreement between the exact solution of Gill's formulation and the Navier–Stokes solution is very good for water, but for air a significant deviation is found. The reason is that the Prandtl number for water is larger than for air, and therefore closer to the infinite-Prandtl-number limit for which the exact solution of Gill's formulation is available. As expected, the deviation from the Navier–Stokes solution is larger for the approximation of Gill's formulation than for the exact solution of Gill's formulation. For water the accuracy of Gill's approximation is still reasonable, but for air the deviation is large. This shows that Graebel's finite-Prandtl-number corrections (which are included in the approximation of Gill's formulation in Table 3) are not very accurate for air. Finally, the averaged wall-heat transfer in Ostrach's similarity solution is much too small due to the negligence of the stratification and the fixing of the outer-edge temperature at $(T_h+T_c)/2$.

7. FOUR ASYMPTOTIC STRUCTURES

In the previous section the asymptotic structure of the Navier–Stokes solution in the vertical boundary layer and in the core was shown to satisfy Gill's asymptotic description. In this section some further details for the vertical boundary layer and the core are given and the structure of the two other asymptotic regions, namely the corner and the horizontal boundary layer, is described. The proper scalings as calculated in the large-Rayleigh-number Navier–Stokes solution are summarized in Table 4.

7.1. *Vertical boundary layer along the heated wall*

The presence of the horizontal walls is felt by the vertical boundary layer via the temperature stratification in the core. Firstly the stable stratification gives small regions with flow reversal and temperature deficit in the outer part of the boundary layer. The flow reversal changes the parabolic character of the boundary-layer solution in an isothermal environment into an elliptic character. Secondly the stable stratification results in mass being moved into the hot boundary layer at heights smaller than $H/2$, and moved out from the boundary layer at larger heights. In Fig. 4 it was shown that the wall-heat transfer in the Navier–Stokes solution for $Ra \to \infty$ satisfies the boundary-layer equations. In analogy, according to the boundary-layer scalings, the x-coordinate, the vertical velocity, and the temperature in the Navier–Stokes solution should scale with $HRa^{-1/4}$, $u_0 Ra^{1/6}$ and ΔT, respectively, in the limit $Ra \to \infty$. The velocity scale $u_0(Ra/Pr)^{1/6} = (g\beta\Delta TH)^{1/2}$ is known as the buoyant velocity scale. The correctness of these scalings is verified for the v-profile at $y = H/2$ for air in Fig. 7(a). The velocity maximum is shown in Fig. 7(b). For small y values the velocity maximum follows Ostrach's similarity solution

$$\lim_{Ra\to\infty} \frac{v_{max}}{\sqrt{(g\beta\Delta TH)}} = C^*\sqrt{(y/H)} \lim_{Ra\to\infty} \left(\frac{T_h - T(H/2,0)}{\Delta T}\right)^{1/2} \tag{10}$$

with $C^* = 0.555$ for air and 0.263 for water. This similarity solution, which assumes an isothermal environment, only moves mass into the boundary layer and the velocity maximum increases with increasing y. No mass is moved out through the outer edge of the boundary-layer as occurs in the case of a stratified environment for $y > H$. Hence, due to the stratification, the velocity maximum deviates from Ostrach's solution for larger y and the velocity maximum is largest at $y \sim H/2$. Reaching $y/H = 1$, the maximum in the boundary-layer solution deviates from the Navier–Stokes solution; the Navier–Stokes solution smoothly falls back to zero, whereas the boundary-layer solution hits the ceiling with a finite velocity maximum. The minimum of the velocity, that is, the maximum of the flow reversal, is

Table 4. Navier–Stokes scalings for the steady laminar flow

Region	Quantity	Scaling	Examples: Quantity	Air	Water
Vertical boundary layer	u	$(g\beta\Delta Tv)^{1/3} Ra^{-1/12}$			
	v	$\sqrt{(g\beta\Delta TH)}$	$\frac{v_{max}}{\sqrt{(g\beta\Delta TH)}} =$	0.27	0.089
	T	ΔT	$\frac{y_{vmax}}{H Ra^{-1/4}} =$	1.2	1.4
	x	$H Ra^{-1/4}$	$\overline{Nu}\, Ra^{-1/4} =$	0.30	0.32
	y	H			
Core	u	$(g\beta\Delta Tv)^{1/3} Ra^{-1/12}$			
	v	$v \ll u$	$\frac{\psi_c}{u_0 H Ra^{-1/12}} =$	0.66	0.16
	T	ΔT			
	x	H	$S =$	0.99	0.55
	y	H			
Corner	T	ΔT	$Nu_{max}\, Ra^{-1/3} =$	0.19	0.24
	y	$H Ra^{-1/3}$	$\frac{y_{Numax}}{H Ra^{-1/3}} =$	3.8	3.9
Horizontal layer	u	$(g\beta\Delta Tv)^{1/3}$			
	v	$v \ll u$	$\frac{u_{max}}{(g\beta\Delta Tv)^{1/3}} =$	0.82	0.24
	T	ΔT			
	x	H	$\frac{y_{umax}}{H Ra^{-3/16}} =$	2.3	1.6
	y	$H Ra^{-3/16}$			

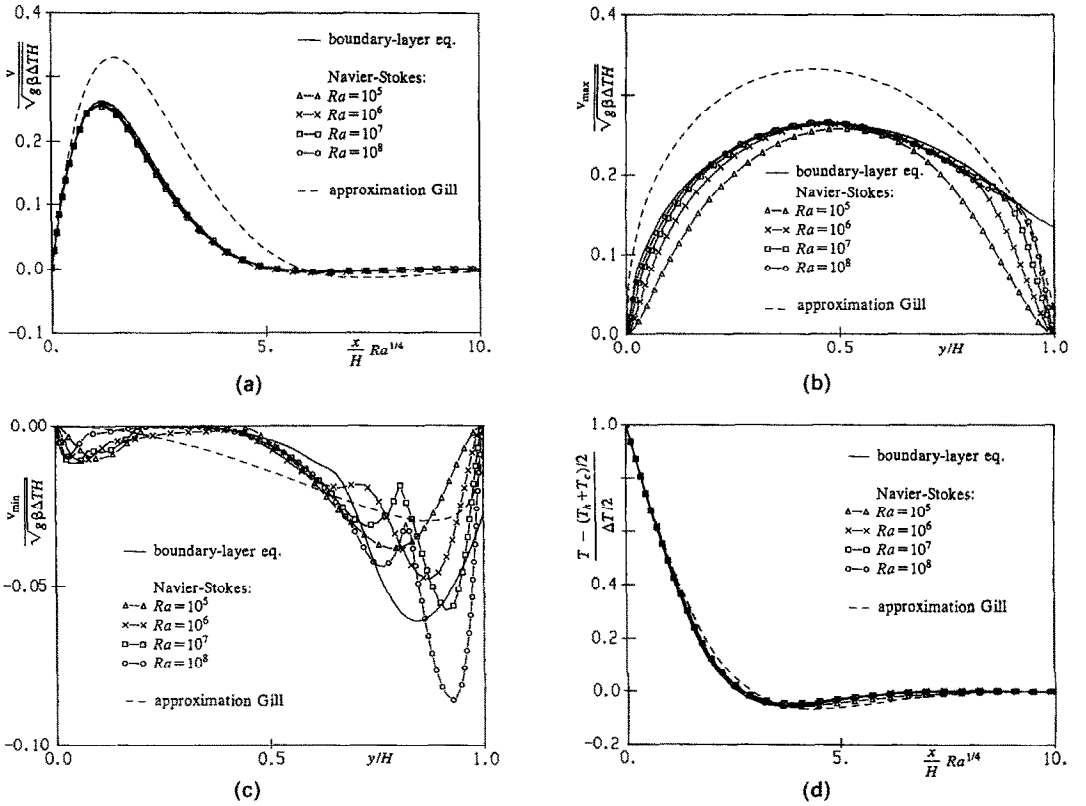

FIG. 7. Vertical boundary layer for air; (a) vertical velocity at $y = H/2$, (b) maximum in the vertical velocity, (c) minimum in the vertical velocity, (d) temperature at $y = H/2$.

shown in Fig. 7(c) for air. Deviations in the minimum between the boundary-layer solution and the Navier–Stokes solutions will be discussed in Section 7.3. The scaling of the temperature profile at $y = H/2$ for air is verified in Fig. 7(d).

7.2. *Core region*

The Navier–Stokes solutions show that for increasing Rayleigh number the temperature becomes stratified in the core and the velocities in the core become much smaller compared to the velocities in the vertical boundary layers. Moreover the streamlines become horizontal in the core. Therefore the core velocities can be fitted to

$$\lim_{Ra\to\infty} \frac{u}{u_0} \doteq Ra^{-a} \quad a > -1/6$$

$$\lim_{Ra\to\infty} \frac{v}{u_0} \doteq Ra^{-b} \quad b > a. \tag{11}$$

The length scale in the core is expected to be H; the horizontal velocity can transport the mass from the hot vertical boundary layer, which is proportional to $u_0 Ra^{1/6} \times HRa^{-1/4}$, to the cold boundary layer if $a = 1/12$. Integration of the horizontal velocities at $x = H/2$ gives the stream function of Fig. 5(a). The scaling with $a = 1/12$ for the horizontal velocity in the core agrees with the boundary-layer scaling for the normal velocity (6) and is checked in Fig. 8(a) for

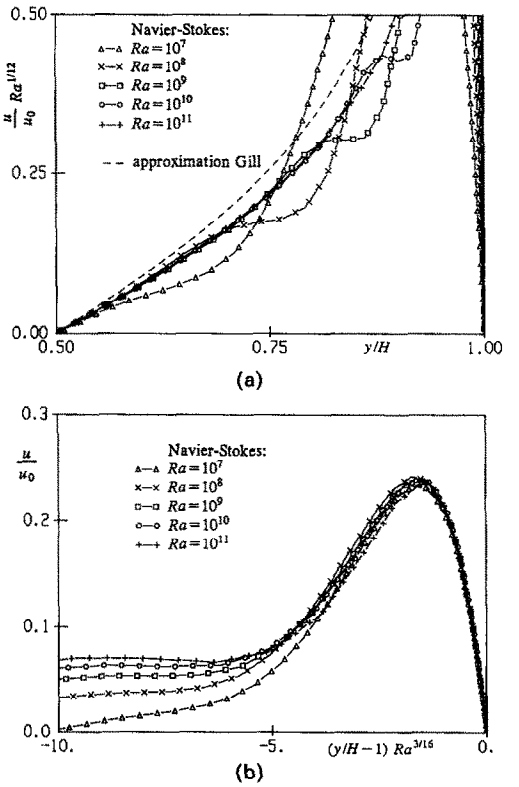

FIG. 8. Horizontal velocity for water at $x = H/2$; (a) in the core, (b) in the horizontal layer.

water. For increasing Rayleigh number the horizontal boundary layers along the horizontal walls become thinner and the core becomes larger. Indeed Fig. 8(a) shows that for increasing Rayleigh number an increasing part of the horizontal velocity falls on a single curve that scales with the velocity $u_0 Ra^{1/12}$. The figure also shows that the scaled horizontal velocity in the core, $(u/u_0)Ra^{1/12}$, becomes infinitely large at $y/H \downarrow 0$ and $y/H \uparrow 1$ for increasing Rayleigh number. Such a growth without bound is also found in the normal velocity at the leading edge of Ostrach's similarity solution. The vertical core velocities are so small that the exponent b in equations (11) cannot accurately be determined from the calculated Navier–Stokes solutions. Nevertheless, it is clear that for large Rayleigh numbers we find $v \ll u$ in the core. The core region for air seems to show the same scaling for the horizontal velocity as for water; for air, however, even the largest calculated Rayleigh numbers still give a rather thick horizontal boundary layer which makes the verification of the scaling for the horizontal core velocity less clear than for water.

7.3. *Corner region*

In the left upper corner the vertically rising boundary layer hits the ceiling with a finite velocity maximum. In this region the flow can no longer be described with boundary-layer equations. No clear scalings can be derived from the large-Rayleigh-number Navier–Stokes solution, implying that full Navier–Stokes equations have to be used in this corner region. Pressure forces become important here and cause the boundary layer to change direction and continue as a horizontal layer. Because for large Rayleigh numbers the vertical boundary layers and the core are described by the boundary-layer equations (4), the pressure plays only a passive role in these regions and reduces to the hydrostatic pressure (5) in the limit $Ra \to \infty$, giving horizontal isobars. Figure 9 shows that the pressure becomes active in the left upper corner (and the right lower corner); for air at $Ra = 10^8$ we have plotted the isobars after subtraction of the hydrostatic pressure with respect to the core stratification ($T_c(y)$ is evaluated at half the cavity width in equation (5)). For air a vortex in the streamline pattern (Fig. 1(a)) characterizes the bending of the vertical layer to the horizontal layer in the corner. The influence of the vortex is also clearly seen in the minimum velocity for air in Fig. 7(c). In the Navier–Stokes solution for $Ra = 10^5$ and $Ra = 10^6$ the vortex is still absent, and the minimum velocity is relatively close to the boundary-layer solution. With the appearance of the vortex at $Ra = 10^7$, a new peak arises in the velocity minimum. It is expected that for increasing Rayleigh number the influence of the vortex disappears and that the Navier–Stokes solution comes closer to the boundary-layer solution. The influence of the vortex on the minimum, however, is still large at $Ra = 10^8$. Figure 4(a) shows that the influence of the left lower corner (the starting corner of the vertical boundary layer) on the wall-heat transfer quickly disappears with increasing Rayleigh number: the position y/H of the maximum in the wall-heat transfer comes closer to the floor. More precisely, its position y turns out to scale with $HRa^{-1/3}(=(g\beta\Delta TPr/\nu^2)^{-1/3})$. This scaling shows that the size of the cavity (H) does not influence the flow structure at the starting corner.

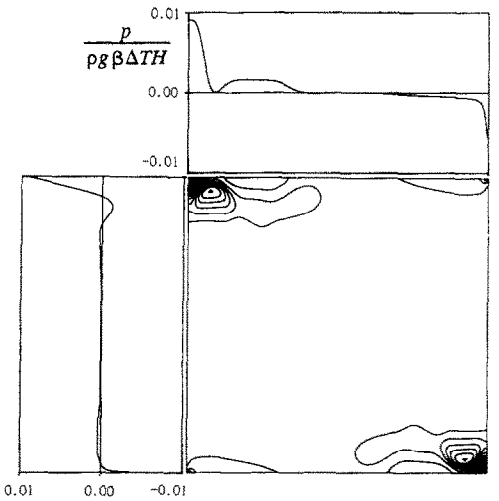

FIG. 9. Pressure, after subtraction of the hydrostatic pressure, for air at $Ra = 10^8$; isobars in the cavity and pressure distribution along the ceiling and along the hot wall.

7.4. *Horizontal layer*

The horizontal boundary layer along the adiabatic horizontal wall is of a different type than the vertical boundary layer: the horizontal boundary layer is not described by the boundary-layer equations (4). The horizontal layer forms the connection between the core flow and the no-slip and adiabatic condition at the horizontal wall. Similarly to the structure in the core, the isotherms and streamlines in the Navier–Stokes solution become horizontal for $Ra \to \infty$. Because the horizontal wall is adiabatic, the horizontal layer is even isothermal (with a temperature below T_h in the horizontal ceiling layer). Considering the u-velocity in Fig. 8(a), the horizontal layer in the y-direction can be said to extend roughly from the horizontal wall up to the velocity maximum. As checked in Fig. 8(b), the y-coordinate and u-velocity scale with $HRa^{-3/16}$ and u_0, respectively. It is remarkable that this velocity scale ($u_0 = (g\beta\Delta T\nu)^{1/3}$) is independent of H. The mass that is transported through the horizontal layer is proportional to $u_0 HRa^{-3/16}$, whereas the mass through the core is proportional to $u_0 HRa^{-1/12}$. This implies that for an infinitely large Rayleigh number all the mass from the hot vertical boundary layer is transported to the cold vertical boundary layer via the core. This agrees with Gill's assumptions about the asymptotic structure.

8. CONCLUSION

The steady laminar Navier–Stokes solution for air and water in the square cavity heated from the vertical side and with an adiabatic floor and ceiling shows four different streamline patterns (topological structures), when the Rayleigh number is increased up to 10^{11}. The last streamline pattern ($Ra > 5 \times 10^6$) contains four asymptotic structures: a vertical boundary layer along the heated wall, a core region, a corner region and a horizontal layer.

For increasing Rayleigh number the core becomes thermally stratified and has horizontal streamlines. The vertical temperature gradient in the centre of the core scales with $\Delta T/H$ and is roughly twice as large for air than for water. The horizontal velocity in the core scales with $(g\beta\Delta Tv)^{1/3}Ra^{-1/12}$. Comparison with the solution of the boundary-layer equations (using the large-Rayleigh-number temperature stratification in the core as a boundary condition) shows that for $Ra \to \infty$ the Navier–Stokes solution along the vertical wall converges to the boundary-layer solution. This means that the wall-heat transfer scales with $(\Delta T/H)Ra^{1/4}$, the vertical velocity with $(g\beta\Delta TH)^{1/2}$ and the boundary-layer thickness with $HRa^{-1/4}$. Finite Rayleigh-number effects in the Navier–Stokes solution for the vertical layers are restricted to influences in the corners. In the left upper corner the vertical boundary-layer solution hits the ceiling with a non-zero maximum speed. For air a vortex characterizes the process of bending the vertical layer to a horizontal layer. No scalings can be derived in the left upper corner, implying that full Navier–Stokes equations have to be used there. The horizontal layers along the horizontal walls are not described by boundary-layer equations. They have horizontal streamlines and are isothermal. The y-distance to the horizontal wall scales with $HRa^{-3/16}$ and the horizontal velocity scales with $(g\beta\Delta Tv)^{1/3}$.

The large-Rayleigh-number structures along the vertical walls and in the core, as calculated with the Navier–Stokes equations and the boundary-layer equations, agree with the asymptotic description proposed by Gill.

REFERENCES

1. J. W. Elder, Laminar free convection in a vertical slot, *J. Fluid Mech.* **23,** 77–97 (1965).
2. A. E. Gill, The boundary-layer regime for convection in a rectangular cavity, *J. Fluid Mech.* **26,** 515–536 (1966).
3. L. Prandtl, Uber Flüssigkeitsbewegung bei sehr kleiner Reibung, *Proc. 3rd Int. Math. Congr.*, Heidelberg (1904). Reprinted in: *Vier Abhandlungen zur Hydro- und Aerodynamik*, Göttingen (1927); NACA TM 452 (1928); see also *Coll. Works* II, pp. 575–584 (1961).
4. S. Ostrach, Natural convection in enclosures. In *Advances in Heat Transfer* (Edited by J. P. Hartnett and T. F. Irvine, Jr), Vol. 8, pp. 161–227. Academic Press, New York (1972).
5. S. Ostrach, Natural convection heat transfer in cavities and cells. *Proc. 7th Int. Heat Transfer Conf.* (Edited by U. Grigull *et al.*), Vol. 1, pp. 365–379 (1982).
6. G. K. Batchelor, Heat transfer by free convection across a closed cavity between vertical boundaries at different temperatures, *Q. Appl. Math.* **12,** 209–233 (1954).
7. S. Ostrach and R. G. Hantman, Natural convection inside a horizontal cylinder, *Chem. Engng Commun.* **9,** 213–243 (1981).
8. A. Bejan, Note on Gill's solution for free convection in a vertical enclosure, *J. Fluid Mech.* **90,** 561–568 (1979).
9. W. P. Graebel, The influence of Prandtl number on free convection in a rectangular cavity, *Int. J. Heat Mass Transfer* **24,** 125–131 (1981).
10. P. A. Blythe, P. G. Daniels and P. G. Simkins, Thermal convection in a cavity: the core structure near the horizontal boundaries, *Proc. R. Soc. Lond.* **A387,** 367–388 (1983).
11. G. de Vahl Davis, Natural convection of air in a square cavity: a benchmark numerical solution, *Int. J. Num. Meth. Fluids* **3,** 249–264 (1983).
12. P. Le Quéré, Accurate solutions to the square thermally driven cavity at high Rayleigh number, *Comput. Fluids* **20,** 29–41 (1991).
13. S. Paolucci and D. R. Chenoweth, Transition to chaos in a differentially heated vertical cavity, *J. Fluid Mech.* **201,** 379–410 (1989).
14. S. Ostrach, An analysis of laminar free-convection flow and heat transfer about a flate plate parallel to the direction of the generating body force, NACA Report 1111 (1953).